Virology 532 (2019) 97–107

Contents lists available at ScienceDirect

Virology

journal homepage: www.elsevier.com/locate/virology

HIV-1 matrix mutations that alter gag membrane binding modulate mature core formation and post-entry events

Yuta Hikichi[a,b,1], Eri Takeda[c,1], Masayuki Fujino[a], Emi Nakayama[c], Tetsuro Matano[a,b], Tsutomu Murakami[a,*]

[a] AIDS Research Center, National Institute of Infectious Diseases, 1-23-1 Toyama, Shinjuku-ku, Tokyo, 162-8640, Japan
[b] The Institute of Medical Science, The University of Tokyo, 4-6-1 Shirokanedai, Minato-ku, Tokyo, 108-8639, Japan
[c] Department of Viral Infections, Research Institute for Microbial Diseases, Osaka University, Suita, Osaka, 565-0871, Japan

ARTICLE INFO

Keywords:
HIV-1
Gag
Matrix
Membrane binding
Core formation
Post entry
Uncoating
Reverse transcription
Integration

ABSTRACT

The matrix (MA) domain of HIV-1 Gag directs membrane binding of the Gag precursor polyprotein during the late events of virus replication. However, the effects of alteration in Gag membrane binding early post-infection are not well understood. To investigate impacts of MA mutations that alter Gag membrane binding on the phenotypes of newly produced virus particles, we extensively characterized two MA mutants by virological, biochemical, and morphological approaches. The V6R mutation, which decreases Gag membrane binding, modified Gag processing and core morphogenesis and impaired core uncoating, reverse transcription, and viral DNA integration. On the other hand, the L20K mutation, which increases Gag membrane binding, primarily decreased integrated DNA levels without affecting the viral components and morphology. These data suggest that HIV-1 MA plays roles in functional core formation and the following post-entry steps of the virus replication cycle. (140/150 words).

1. Introduction

HIV-1 Gag plays important roles in the replication cycle of the virus. Gag is expressed as a 55 kDa polyprotein ($Pr55^{Gag}$), consisting of four domains, namely, matrix (MA), capsid (CA), nucleocapsid (NC), and p6, and of two short spacer peptides, SP1 and SP2 (Freed, 2015; Lingappa et al., 2014). Several lines of evidence indicate that HIV-1 MA has important roles in late events of the HIV-1 replication cycle. The MA domain has been reported to be associated with $Pr55^{Gag}$ membrane binding (Ono and Freed, 1999) and targeting to the plasma membrane in the infected cells (Ono et al., 2000) and incorporation of the Env glycoprotein into virus particles (Tedbury et al., 2015, 2016). Although the detailed structure of full-length $Pr55^{Gag}$ is still unknown, MA is thought to fold into a highly globular structure and form a trimer-of-hexamer complex within virions (Hill et al., 1996; Massiah et al., 1994; Alfadhli et al., 2009; Tedbury et al., 2016). It has been shown that a highly basic region at the top of MA interacts electrostatically with negatively charged lipids on the inner leaflet of the plasma membrane (Dalton et al., 2007), in particular phosphatidylinositol-(4,5)-bisphosphate [PI(4,5)P2] (Ono et al., 2004; Saad et al., 2006). The N-terminus of MA, which is co-translationally modified with a covalently attached myristate moiety, is essential for interaction between Gag and the plasma membrane (Saad et al., 2006; Tang et al., 2004). NMR and biochemical studies indicate that mutations near the N-terminus of MA, such as V6R or L7A, caused structural changes in the N-terminus of MA that resulted in sequestering the myristate moiety and impairing membrane binding of $Pr55^{Gag}$ (Freed et al., 1994; Ono et al., 1997; Ono and Freed, 1999; Saad et al., 2007).

After membrane binding, Gag multimerizes via the CA domain. The CA-CA interaction is the driving force to assemble and release the immature virions from the infected cells (Robinson et al., 2014; Tanaka et al., 2016). During or shortly after budding, the viral protease cleaves Gag in an ordered cascade (Konvalinka et al., 2015), leading to structural rearrangement of the viral Gag proteins to form the mature infectious particle. Although the mechanism of formation of the mature HIV-1 core is still under investigation, three models have been proposed: 1) the disassembly/reassembly model in which free CA monomer produced by cleavage by the viral protease reassembles to form conical cores *de novo* (Briggs et al., 2009; Woodward et al., 2015); 2) the displacive model in which the viral protease induces a sterical

* Corresponding author.
E-mail addresses: yhikichi0@niid.go.jp (Y. Hikichi), etakeda@biken.osaka-u.ac.jp (E. Takeda), fmasa@nih.go.jp (M. Fujino), emien@biken.osaka-u.ac.jp (E. Nakayama), tmatano@nih.go.jp (T. Matano), tmura@nih.go.jp (T. Murakami).
[1] Equally contributed.

https://doi.org/10.1016/j.virol.2019.04.013
Received 29 March 2019; Received in revised form 24 April 2019; Accepted 25 April 2019
Available online 27 April 2019
0042-6822/

transition of CA layers to form conical cores (Frank et al., 2015); and 3) a combination of disassembly/reassembly and displacive models (Ning et al., 2016). Ning et al. and Woodward et al. imply that the viral envelope membrane, the ribonucleoprotein complex and MA guide the growth of conical cores. These models raise the possibility that the membrane binding ability of HIV-1 Gag, which is regulated by MA, influences the formation of the mature cores.

Several studies suggest that HIV-1 MA plays important roles in not only the late stages but also the early stages of the virus replication cycle. A couple of reports have shown that MA is associated with the reverse transcription complex (RTC) or preintegration complex (PIC) (Bukrinsky et al., 1993; Miller et al., 1997). In addition, the L20K mutation in the highly basic patch of MA, which increases membrane binding of Gag, causes defects in single-cycle infectivity and endogenous reverse transcription (ERT) activity without affecting virus morphology (Kiernan et al., 1998). These observations raise the possibility that MA mutations, which alter Gag membrane binding, affect post-entry steps of the HIV-1 replication cycle. However, effects of the MA mutations on core morphogenesis and details of the post-entry process remain to be fully understood largely because experimental techniques to examine these issues were not available at that time.

To obtain insights into the impact of MA mutations that alter Gag membrane binding on the properties of newly produced HIV-1 particles, we extensively characterized two previously reported MA mutants, V6R (Freed et al., 1994) and L20K (Kiernan et al., 1998), along with the V6R revertant V6R/K97E (Ono et al., 1997). To analyze the late events of the HIV-1 replication cycle, we examined virus production, Gag processing, vRNA encapsidation into virions, morphology of the virus particles and mature cores, and endogenous reverse transcription in the virions. To investigate the early events, we measured the infectivity of produced virions, viral cDNA synthesis in late reverse transcription, nuclear import, and integration processes as well as *in situ* uncoating in the virus-infected cells. The L20K mutation decreased integrated DNA in the infected cells without showing effect on the morphology of virus particles or mature cores. On the other hand, the V6R mutation caused the formation of mature cores that were larger than those of the WT, and accelerated the kinetics of uncoating and impaired reverse transcription and integration in the next round of infection. These data suggest that HIV-1 MA may modulate the structural rearrangement of viral cores after Gag processing and the post-entry steps in the virus replication cycle through its membrane binding ability.

2. Materials and Methods

2.1. Cells

HEK293T and TZM-bl cells (Derdeyn et al., 2000; Platt et al., 2009, 1998; Takeuchi et al., 2008; Wei et al., 2002) were maintained in Dulbeccos' modified Eagle medium (DMEM) containing 10% FBS. HeLa cells were maintained in DMEM containing 5% FBS. H9/H1luc cells (Nagao et al., 2004) and Jurkat cells were maintained in RPMI1640 containing 10% FBS.

2.2. Preparation of VSV-G pseudotyped viruses

HEK293T cells were plated (7.0×10^6 cells) on a T-75 cm^2 flask in 15 ml of the medium. Following a day, 10 μg of pNL-Nh (Sakuragi et al., 2003) or MA mutant plasmids (V6R/K97E and L20K) and 2 μg of pHCMV-G (Yee et al., 1994) were transfected into the cells by the calcium phosphate precipitation methods (Ohishi et al., 2007). For V6R mutant, 10 μg of pNL-Nh V6R and 1 μg of pHCMV-G were transfected into the cells. 6 h after transfection, the supernatant was replaced with fresh medium twice. 26 h after transfection, the culture supernatant was harvested and clarified through 0.45-μm-pore filter (Millipore). Following clarification, the culture supernatant was overlaid 20% sucrose/PBS (v/v) and centrifuge at 4 °C at 35,000 rpm for 1 h 30 min using SW41Ti roter. The pellets were resuspended in PBS and aliquots of the viral stocks were stored at −80 °C. The p24 antigen contents were determined by using HIV-1 p24 antigen enzyme-linked immunosorbent assay (ELISA) kit (Zeptometrix) according to manufacturer's instructions. The incorporation of VSV-G into the virus was confirmed by Western blot analysis using *anti*-VSV-G mAb (SIGMA).

2.3. Preparation of NL4-3 and MA mutant viruses

HEK293T cells were plated (7.0×10^6 cells) on a T-75 cm^2 flask in 15 ml of the medium. Following a day, 10 μg of pNL4-3 (Adachi et al., 1986) or MA mutant plasmids (V6R, L7E, S8A, V6R/K97E and L20K) (Freed et al., 1994; Kiernan et al., 1998; Ono et al., 1997; Ono and Freed, 1999) into the cells by the calcium phosphate precipitation methods. 6 h after transfection, the supernatant was replaced with fresh medium. 48 h after transfection, the culture supernatant was harvested and clarified through 0.45-μm-pore filter (Millipore). Following clarification, the culture supernatant was overlaid 20% sucrose/PBS (v/v) and centrifuge at 4 °C at 35,000 rpm for 1 h 30 min using SW41Ti roter. The pellets were resuspended in 5 × sample buffer (300 mM Tris-HCl pH 6.8, 10% SDS, 500 mM DTT and 50% glycerol) or PBS and performed Western blot analysis and natural endogenous assay.

2.4. Single-round infection assay

TZM-bl cells were plated in 96-well plates at 1.0×10^4 cells per well in a volume of 100 μl a day before infection. The cells were infected with serial diluted VSV-G pseudotyped viruses (0.01–2.5 ng/well). For H9/H1luc cells, the cells were plated in 96 well plates at 6.0×10^4 cells per well in a volume of 100 μl and infected with serial diluted VSV-G pseudotyped viruses (0.01–2.5 ng/well). 48 h after infection, luciferase activity was measured using the Steady-Glo Luciferase Assay system (Promega). Luminescence was detected using a Veritas Microplate Luminometer (Promega).

2.5. Viral infection and DNA isolation

Prior to infection, VSV-G pseudotyped viruses were treated with 100U of DNase I (Takara) at 37 °C for 40 min. For HeLa cells, 2.4×10^5 cells were exposed with DNase I-treated VSV-G pseudotyped viruses containing 11.5 ng of p24 and placed at 4 °C for 30 min as synchronization of entry. Following synchronization, the cells were incubated at 37 °C for 3, 6, 9, 24, 48, 72 h. For Jurkat cells, 1.0×10^6 cells were exposed with DNase I-treated VSV-G pseudotyped viruses containing 50 ng of p24 and placed at 4 °C for 30 min. Following synchronization, the cells were incubated at 37 °C for 3, 6, 9, 24, 48 h. At the indicated times, total DNA was extracted from the infected cells using QIAmp DNA blood mini kit (Qiagen) and measured viral DNA by Realtime PCR analysis. As a negative control, VSV-G pseudotyped viruses were heat-inactivated at 65 °C for 30 min.

2.6. Realtime PCR

Realtime PCR was performed with Opticon2 (Biorad) and ABsolute QPCR mix (Thermo scientific). The cycling conditions were as follows: an initial denature step (95 °C、15 min) and 40 cycles of denature steps (95 °C, 15 s) and extension steps (60 °C, 1 min). HIV-1 LTR-Gag/F (5′-GAGATCCCTCAGACCCTTTTAGT-3′) and HIV-1 LTR-Gag/R (5′-AGGACTCGGCTTGCTGAA-3′) and HIV-1 LTR-Gag/probe (5′-FAM-AGTGTGGAAAATCTCTAGCAGTGGCGC-TAMRA-3′) were used for detection of the U5/Gag region of late reverse transcription products. 2-LTR S (5′-CCCTCAGACCCTTTTAGTCAGTG-3′) and 2-LTR AS (5′-TGGTGTGTAGTTCTGCCAATCA-3′) and 2-LTR-FAM probe (5′-FAM-TGTGGATGCTACCACACACAAGGCTACTTCC-TAMRA-3′) were used for detection of 2-LTR circles. huBG/F (5′-CCTGAAGTTCTCAGG ATCCACG-3′) and huBG/R (5′-CAAGAAAGTGCTCGGTGCCTT-3′) and

beta-globin/probe (5′-FAM-ACACTGAGTGTGCTGCACTGTGACAAG CTG-TAMRA-3′) were used for detection of β-Globin. For normalization, β-Globin signal was quantified and the data were shown as the ratio of late RT products or 2-LTR to β-Globin. For quantification of integrated DNA, nested PCR were performed with modifications.(Butler et al., 2001; Hori et al., 2013; Suzuki et al., 2003). The 1st PCR were carried out using PrimeSTAR HS DNA polymerase (Takara) with Alu-HIV (5′-TCCCAGCTACTCGGGAGGCTGAGG-3′) and M661 (5′-CCTGCG TCGAGAGATCTCCTCTG-3′). The cycling conditions of 1st PCR were as follows: an initial denature step (98 °C, 10 s), 22 cycles of denature steps (98 °C, 5 s) and extension steps (72 °C, 10 min). The 1st PCR product was diluted 10-fold and used as template for measuring R/U5 DNA using M667 primer (5′-GGCTAACTAGGGAACCCACTGC-3′) and AA55 primer (CTGCTAGAGATTTTCCACACTGAC-3′) and HIV-FAM probe (5′-FAM-TAGTGTGTGCCCGTCTGTTGTGTGAC-TAMRA-3′).

2.7. Realtime RT-PCR

Viral RNAs were extracted from DNase I-treated VSV-G pseudotyped viruses containing 10 ng of p24 with NucleoSpin RNA Virus kit (Takara). Realtime RT-PCR analysis was performed with Opticon2 (Biorad) as previously described (Ohishi et al., 2011). For detection of viral RNA, TM-GagF (5′-GCAGCCATGCAAATGTTAAAAGAG-3′) and TM-GagR (5′-TCCCCTTGGTTCTCTCATCTGG-3′) were applied with One Step SYBR Prime Script PLUS RT-PCR kit (Takara). The cycling condition was as follow: a reverse transcription step (42 °C, 5 min and 95 °C, 10 s) and 40 cycles of denature steps (95 °C, 5 s) and extension steps (60 °C, 20 s).

2.8. Natural endogenous RT assay

Natural endogenous RT assay was performed with detergent-free method with minor modifications (Thomas et al., 2011; Warrilow et al., 2008). DNase I-treated viruses containing 10 ng of p24 were suspended with PBS (−) and placed on ice. 10 × ERT reaction solution (500 mM Tris-HCl (pH 8.0), 20 mM $MgCl_2$, 10 mM DTT, and 250 μM of each deoxynucleotides) were added into viral solution and placed on ice, then incubated at 37 °C for 3 h. Following incubation, the samples were placed on ice for 3 min. Viral DNA was extracted with QIAmp DNA blood mini kit (Qiagen) and measured R/U5 DNA by Realtime PCR analysis. A dNTP-free sample and no-incubated sample were always included.

2.9. Exogenous RT assay

Exogenous RT assay were performed with minor modification (Willey et al., 1988). Briefly, purified NL4-3 and MA mutant viruses were incubated with 6 × RT cocktail (60 mM Tris-HCl pH7.8, 75 mM KCl, 5 mM $MgCl_2$, 0.1% Igepal CA-630, 1.0 mM EDTA. 5 μg/ml poly A, 0.16 μg/ml oligo dT and 32P-dTTP) for 1 h 30 min. Following incubation, the reaction solution was transferred to DEAE filtermats. The filtermats were washed with SSC buffer for 5 min twice and 100% EtOH once. Meltilex solid scintillator (PerkinElmer) were melted onto the filtermats and RI activities were measured with Microbeta scintillation counter (PerkinElmer). The data were shown as the ratio of RT activity to p24.

2.10. In vitro core disassembly assay

In vitro disassembly assay was performed by a minor modification of the spin-thru method (Aiken, 2009; Shah and Aiken, 2011). Briefly, HEK293T cells were plated (7.0×10^6 cells) on a T-75 cm^2 flask in 15 ml of the medium. Following a day, 10 μg of pNL4-3, MA mutant plasmids (V6R, V6R/K97E, L7E, S8A and L20K) or CA mutant plasmids (Q63A/Q67A, E128A/R132A and E45A) (Forshey et al., 2002; von Schwedler et al., 2003) into the cells by the calcium phosphate precipitation methods. 6 h after transfection, the supernatant was replaced with fresh medium. 48 h after transfection, the culture supernatant was harvested and clarified through 0.45-μm-pore filter (Millipore). Following clarification, the culture supernatant was overlaid 20% sucrose/PBS (v/v) and centrifuge at 4 °C at 32,000 rpm for 2 h using SW32Ti roter. The pellet was resuspended with 1 × STE buffer (10 mM Tris-HCl (pH7.5), 100 mM NaCl, 1 mM EDTA). Virus suspension was overlaid 1.5% sucrose in STE buffer containing 1% Triton X-100, which had been placed on top of a linear gradient of 30%–70% sucrose in STE buffer. To prevent mixing virus suspension and detergent layer, 7.5% sucrose/STE buffer was inserted between these layers. Concentrated virus suspension was centrifuged at 4 °C at 35,000 rpm for 18 h using SW41Ti roter. Following centrifugation, the gradients are fractionated from top of the gradient. The density of each fraction was measured by refractometry and was subjected to SDS-PAGE and Western blot analysis. The fraction containing cores (1.23–1.26 g/ml) diluted and incubated at 37 °C or 4 °C for 2 h. Following incubations, the dilutions were centrifuge at 4 °C at 20,000 × *g* for 1 h 30 min. To determine the core stability, pellet fractions were subjected to SDS-PAGE and Western blot analysis.

2.11. Western blot analysis

The viral proteins were separated by SDS-PAGE and transferred to polyvinylidene disulfide (PVDF) membranes (Millipore). Membranes were probed with primary antibody at room temperature for 1 h, and incubated for 30 min with species-specific biotinylated secondary antibody (GE healthcare). After incubation, the membranes were incubated at room temperature for 30 min. After washes, bands were detected by LAS3000 mini (GE healthcare) using Amersham ECL SELECT Western Blotting Detection Reagent (GE healthcare) or Lumi-Light Western Blotting Substrate (Roche). p24 protein was detected with *Anti*-HIV-1 serum obtained from the NIH AIDS Reagent program or p24 monoclonal antibody (13-102-100: Advanced Biotechnologies Inc.). p17 protein was detected with *anti*-p17 monoclonal antibody (13-103-100: Advanced Biotechnologies Inc.). RT proteins were detected with 7C4 monoclonal antibody (Chiba et al., 1996). IN was detected with *anti*-HXB2 IN 1–16 aa polyclonal antibody obtained from the NIH AIDS Reagent program (Bukrinsky et al., 1993; Grandgenett and Goodarzi, 2008). CypA was detected with *anti*-CypA serum (Thermo scientific).

2.12. In situ uncoating assay

The *in situ* uncoating assay was conducted as previously described (Campbell et al., 2007; Kono et al., 2013; Yamashita et al., 2007). Briefly, 2.2×10^5 HeLa cells were infected with viral titers equivalent to 100 ng of p24 of VSV-G-pseudotyped fluorescent labeled wild type and mutant viruses with GFP-Vpr and S15-dTomato. the labeled virus was generated by cotransfecting 9 μg NL-Nh mutant proviral plasmid, 4 μg S15-dTomato-expressing plasmid, 4 μg vesicular stomatitis virus G protein (VSV-G)-expressing plasmid, and 1 μg GFP-Vpr expressing plasmid into 5×10^6 of 293T cells using polyethylenimine (PEI) (molecular weight, 25,000; Polysciences). At 2 days posttransfection, culture media was collected and filtrated with 0.45 μm filter. Viral titers were determined with the RETROtek antigen ELISA kit (ZeptoMetrix, Buffalo, NY). HeLa cells in 24-well plate were spinoculated with the labeled virus for 2 h at 16 °C in the presence or absence of bafilomycin A (BAF) (Sigma). Virus-containing supernatant then was removed and replaced with 37 °C medium in the presence or absence of BAF, shifted to 37 °C, and fixed with 3.7% formaldehyde (Polysciences) in 0.1M PIPES buffer (pH 6.8) at the indicated time point post-infection. The fixed HeLa cells were permeabilized with blocking solution (PBS, 10% normal donkey serum [Jackson ImmunoResearch Laboratories], 0.01% Triton X-100, 0.01% NaN3) for 5 min at room temperature, stained with *anti*-p24 mAb AG3.0 (NIH AIDS Research and Reference Reagent

Program) in blocking solution without Triton X-100 for 1 h at room temperature for primary staining, and secondarily stained with labeled Cy-5 donkey anti-mouse antibodies (Jackson ImmunoResearch Laboratories) for 30 min at room temperature. Images were collected and deconvolved with an Eclipse TE2000-E inverted microscope and NIS-Elements AR software (Nikon). Following deconvolution, images were blinded for identity to remove bias during counting. The number of GFP-positive virions was assessed at each time point, and each virion was individually inspected for punctate dTomato fluorescent signal and p24 Cy-5 signal.

2.13. Transmission electron microscopy (TEM)

Viral cores were isolated as previously described in Accola et al. (2000). After ultracentrifugation, viral cores were reconstituted and fixed with 0.1 M phosphate buffer containing 1.3% glutaraldehyde. These were absorbed onto Formvar-coated copper grids, and staining uranyl acetate. The images were recorded with a JEM-1011 transmission electron microscopy (JEOL) and the lengths and widths of viral cores were measured.

2.14. Statistical analysis

Statistical analyses were performed with Graphpad Prism version 5 (Graphpad software Inc.). Deference between WT and MA mutants were examined by one-way analysis of variance (ANOVA) and Turkey-Kramer's multiple-comparison test. Asterisk indicates *P* value (*: 0.01 to 0.05, **: 0.001 to 0.01, ***: < 0.001).

3. Results

3.1. The V6R and L20K MA mutations do not significantly affect the composition of virus particles

Previous studies showed that a V6R mutation in HIV-1 MA impairs virus production whereas a L20K mutant does not affect virus release in HeLa cells (Freed et al., 1994; Kiernan et al., 1998; Ono et al., 1997). We first examined the amounts of p24 CA antigen in the culture supernatants of transfected 293T cells, and found that the V6R and L20K mutants produced about a half or comparable levels of virus particles, respectively compared with pNL4-3 (WT) (data not shown). The viral protein composition in the cell and viral lysates was also examined by Western blot analysis. Impaired or enhanced $Pr55^{Gag}$ processing was observed for the V6R and L20K mutant, respectively (Fig. 1A) in cell lysates. In contrast, Pol processing, indicated by the amounts of p66/p51 (reverse transcriptase, RT), integrase (IN), and the incorporation of the host protein cyclophilin A (CypA) in virions were not significantly affected by the MA mutations (Fig. 1B). We also examined viral RNA encapsidation and levels of virion-associated RT activity using real-time RT-PCR and exogenous RT assay, respectively. The V6R, V6R/K97E (a revertant for V6R) (Ono et al., 1997), and the L20K virions contained WT levels of viral RNA and RT activity when they were normalized by p24 CA antigen amount (Fig. 1C and D). These results indicate that the V6R and L20K mutations in MA do not significantly affect viral protein composition, genomic viral RNA and RT activity in virions.

3.2. Single-cycle infectivity assays of the MA mutants show a post-entry defect(s) in the HIV-1 replication cycle

To determine whether an early phase in the HIV-1 replication cycle is influenced by the V6R mutation, a single-cycle infectivity assay was performed using TZM-bl cells as a target cell line. The results indicated that the V6R mutation caused 5- to 10- fold reduction in virus infectivity as did the L20K mutation as reported previously (Kiernan et al., 1998) (data not shown), suggesting that both MA mutations affect early steps of the virus replication cycle.

It is known that pseudotyping with an envelope protein of other viruses, such as the vesicular stomatitis virus G glycoprotein (VSV-G), enables some HIV-1 mutants to bypass early post-entry defects (Aiken, 1997). To investigate whether pseudotyping with VSV-G rescues the defects caused by the MA mutations, we compared viral infectivity of VSV-G pseudotyped MA mutants using TZM-bl cells and H9/H1luc cells as targets. To normalize the efficiency of viral entry, we confirmed that all of MA mutants contain comparable levels of VSV-G by Western blot analysis before viral infection (data not shown). As previously reported (Kiernan et al., 1998), the impaired infectivity of the L20K mutant was not rescued by VSV-G pseudotyping in TZM-bl or H9/H1 cells (Fig. 2A and B). The infectivity defect imposed by the V6R mutation was not reversed by VSV-G pseudotyping in either cell types whereas the infectivity of the V6R/K97E revertant was nearly comparable to that of WT in TZM-bl and partially restored in H9/H1luc cells (Fig. 2A and B, respectively). These results suggest that the V6R and L20K mutations cause a defect(s) in the post-entry steps of the virus replication cycle and that in the case of V6R a single-amino acid change can rescue the defect by restoring Gag membrane binding (Ono and Freed, 1999).

3.3. V6R impairs HIV-1 cDNA synthesis and L20K reduces the levels of integrated viral DNA

We next analyzed the impact of the MA mutations on the early stages of HIV-1 replication using quantitative real-time PCR. HIV-1 cDNA including late reverse transcribed (late RT) viral cDNA products and integrated form of proviral DNA were measured in HeLa cells infected with VSV-G pseudotyped viruses. The V6R mutant exhibited a minor defect in reverse transcription although the defect is not statistically significant (Fig. 3A and C). Meanwhile, the level of integrated proviral DNA for this mutant was significantly reduced compared with WT (Fig. 3B and C). In the V6R/K97E revertant, these two defects were mostly reversed. On the other hand, the L20K mutant exhibited comparable levels of the late RT viral cDNA synthesis relative to WT, but showed a defect in the level of integrated proviral DNA (Fig. 3A, B and 3C). We next performed real-time PCR using a more physiologically relevant cell type, Jurkat T-cell line. In Jurkat cells, the V6R mutation significantly reduced RT efficiency, resulting in impaired levels of the integrated form of the viral DNA (Fig. 3D, E and 3F). The V6R/K97E reversed the defects imposed by the V6R mutation. As we observed in HeLa cells, the L20K mutation did not affect levels of the late RT viral cDNA, but reduced the level of the integrated form of the proviral DNA (Fig. 3A, B and 3C). Importantly, the levels of the integrated form of the viral DNA in HeLa and Jurkat cells correspond to the infectivities of the MA mutants in TZM-bl cells and H9/H1 cells. Next, to investigate the efficiency of nuclear import of the viral DNA, we measured the levels of 2-LTR circles, which are unproductive viral DNA forms in the nucleus of the infected cells. Although the V6R mutant impaired RT efficiency, it displayed about 200% of the WT 2-LTR circles level when 2-LTR circles were normalized to the quantity of the late RT products (Fig. 4, closed bars). Some reports indicate that defects in integration induce accumulation of 2-LTR in the nucleus (J Buzón et al., 2010; Svarovskaia et al., 2004). Thus, it is difficult to distinguish between the integration defects and acceleration of nuclear import. To more directly quantify the efficiency of nuclear import, we compared the levels of 2-LTR circles of the MA mutants in the presence or absence of an integrase inhibitor, raltegravir (RAL). In control experiments, the level of 2-LTR circles detected with WT increased up to about 4-fold in the presence of RAL (Fig. 4A). Under such experimental conditions, the levels of 2-LTR circles of the MA mutants including V6R were comparable to those of WT in the presence of RAL (Fig. 4), suggesting that the V6R mutation does not affect the nuclear entry process. Collectively, these results suggest that the V6R mutation in MA impairs both viral cDNA synthesis and integration, thereby reducing the level of the proviral DNA in target cells.

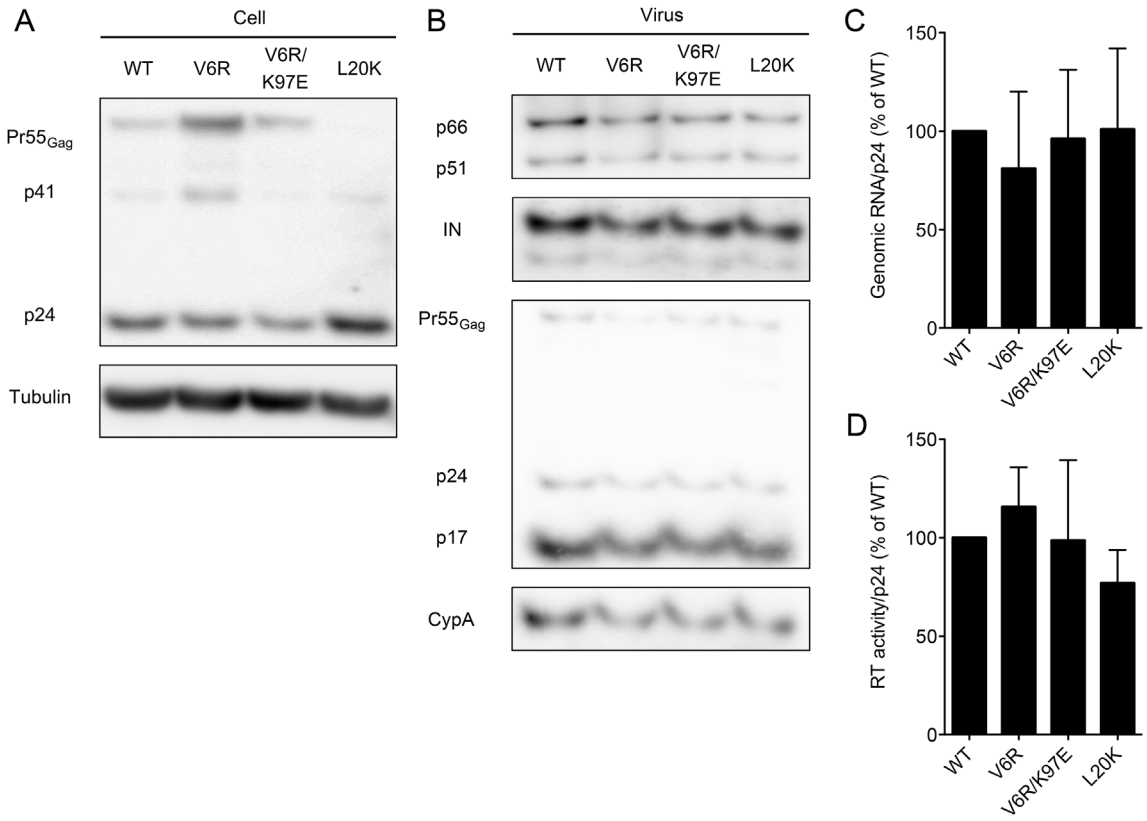

Fig. 1. Analysis of WT and CA mutant viral components in cell lysates and in virions. 293T cells were transfected with WT HIV-1 (NL4-3) or MA mutant viruses. (A) Cell-associated proteins were probed with AIDS patient serum or anti-tubulin antibodies for Western blot analysis. (B) Normalized amounts of virions present in culture supernatant were probed with *anti*-RT or anti-IN or a mixture of *anti*-p24 and *anti*-p17 or *anti*-CypA antibodies. The panel A and B images are the representative of results obtained from at least three independent experiments. (C) RNA was extracted from DNase I-treated virions and analyzed by quantitative RT-PCR using primers specific for HIV-1 sequences. Results shown are the average of four independent experiments, with error bars representing standard deviations. (D) Exogenous RT activities of virions were measured as described in "Materials and Methods" and normalized for p24 antigen amounts. Results shown are the average of three independent experiments, with error bars representing standard deviations.

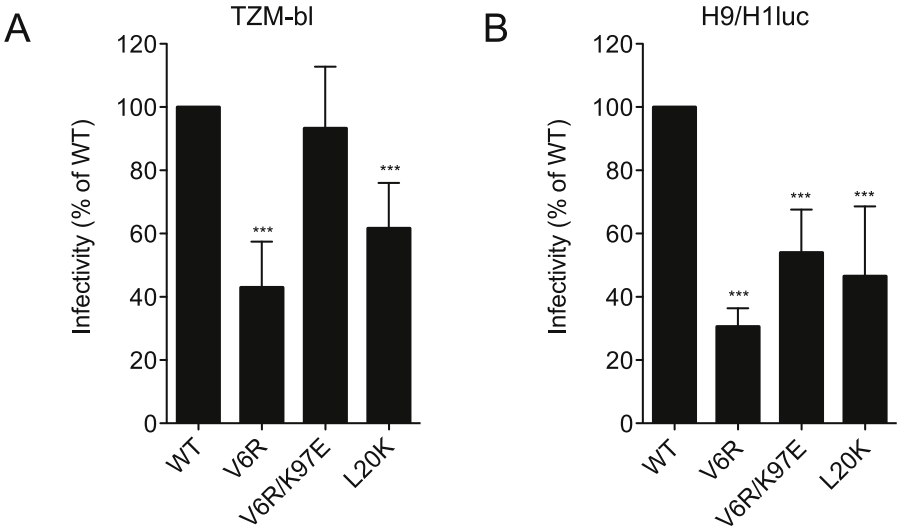

Fig. 2. Effect of HIV-1 MA mutations on viral infectivity. Normalized amounts of VSV-G pesudotyped WT HIV-1 (NL4-3) or MA mutant viruses were infected in TZM-bl cells (A) or H9/H1luc cells (B). The cells were harvested and subjected to determination of luciferase activities at 48 h postinfection. Results shown are the average of at least four independent experiments, with error bars representing standard deviations. Values are significantly different as follows: *, $P = 0.01$ to 0.05, **, $P = 0.001$ to 0.01, ***, $P < 0.001$.

3.4. The V6R mutation accelerates the kinetics of uncoating

Several lines of evidence suggest that HIV-1 reverse transcription occurs before or during uncoating, and these two events are linked to each other in the early steps of the virus replication cycle (Cosnefroy et al., 2016; Forshey et al., 2002; Hulme et al., 2011; Rankovic et al., 2017; Yang et al., 2013). Therefore, we next addressed the question whether the MA mutations affect disassembly of the capsid core complex in the target cell by performing *in situ* uncoating assays (Campbell et al., 2007; Kono et al., 2013; Yamashita et al., 2007). Briefly, HeLa cells were infected with VSV-G pseudotyped, fluorescently labeled WT and MA mutants containing Vpr fused with green fluorescent protein (GFP-Vpr) and S15-dTomato. At various time points (0, 1, 2, and 4 h) after infection, the cells were fixed and immunostained for p24 CA (Cy-5). Total number of complexes that entered and fused in the cytoplasm (Vpr-GFP$^+$, S15-dTomato$^-$), the number of complexes

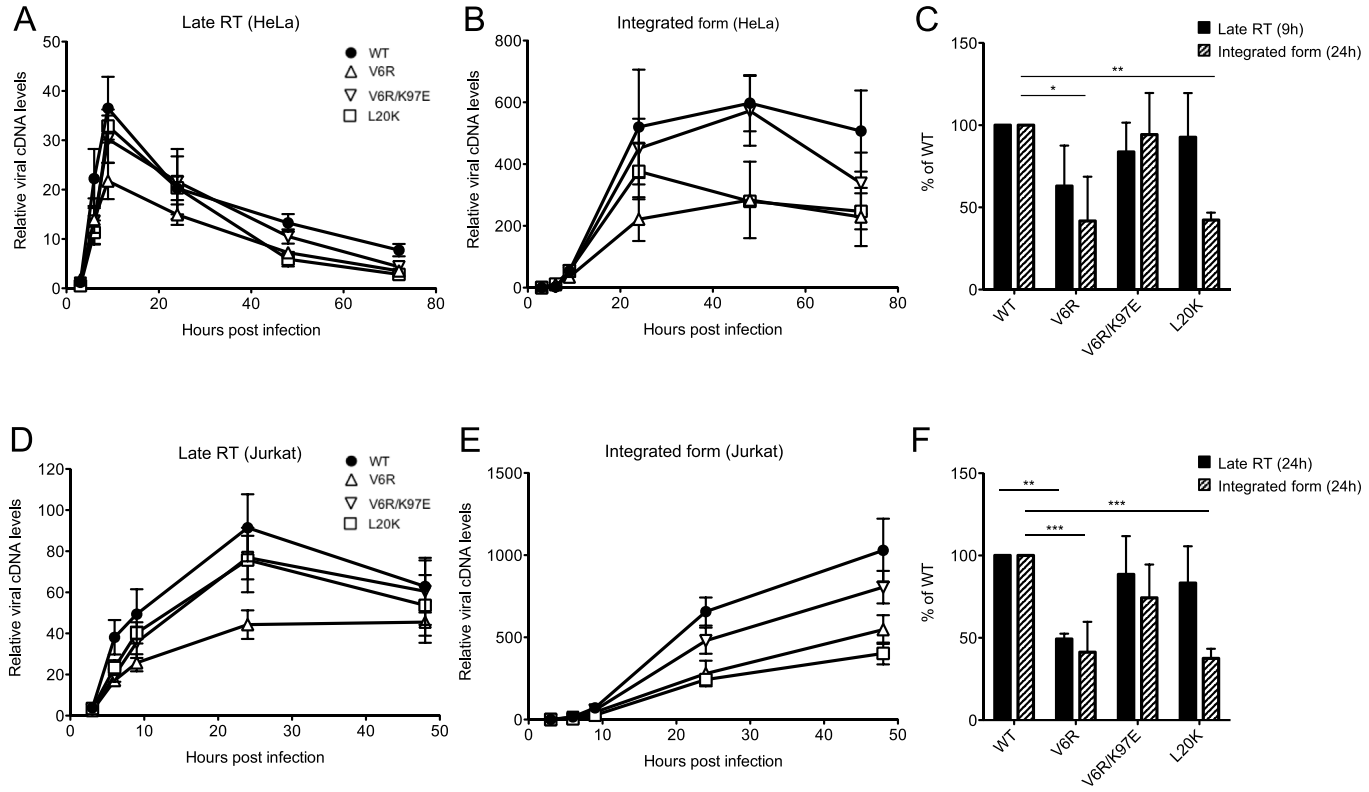

Fig. 3. Effect of HIV-1 MA mutations on the synthesis of viral DNA in HeLa cells or Jurkat cells. (A to C) HeLa cells were infected with VSV-G pseudotyped WT and MA mutant viruses. The DNA was extracted at 3, 6, 9, 24, 48, and 72 h after infection and subjected to real-time PCR using U5/gag primers for late reverse transcription products (A), and Alu-primers for integrated DNA (B). The level of each mutant is indicated relative to the average values of the WT virus, which was set as 100% (C). Error bars reflect the standard errors (A and B) and the standard deviations (C) of at least three independent experiments, respectively. (D to F) Jurkat cells were infected with VSV-G pseudotyped WT and MA mutant viruses. The DNA was extracted at 3, 6, 9, 24, and 48 h after infection and subjected to real-time PCR using U5/gag primers for late reverse transcription products (D), and Alu-primers for integrated DNA (E). The level of each mutant is indicated relative to the average values of the WT virus, which was set as 100% (F). Error bars reflect the standard errors (D and E) and the standard deviations (F) of at least three independent experiments, respectively. Values are significantly different as follows: *, $P = 0.01$ to 0.05, **, $P = 0.001$ to 0.01, ***, $P < 0.001$.

containing CA (Vpr-GFP$^+$, CA-Cy5$^+$), and the number of complexes lacking CA that lost CA staining (Vpr-GFP$^+$, CA-Cy5$^-$) were counted. Bafilomycin A (BAF) was added to one sample as a negative control for fusion. The data are presented at each time point as the percentage of the coated particles in the total fused GFP + particles. The V6R mutant showed accelerated kinetics of CA disassembly, whereas uncoating kinetics of V6R/K97E and L20K were similar to those of WT (Fig. 5).

3.5. The size of V6R viral cores is bigger than that of WT

Although the V6R mutation in MA does not significantly affect viral components in virions, this mutation causes impaired reverse transcription and accelerated uncoating in virus-infected cells. Therefore, we then analyzed morphology of the MA mutant virions and viral cores prepared by detergent treatment and isolation of the virions. By transmission electron microscopy (TEM) analysis, we observed that the two MA mutants (V6R and L20K) as well as V6R/K97E produced mature virus particles that contain cone-shaped cores as did WT. The virion size of V6R mutant was somewhat larger than WT and V6R/K97E (data not shown). We next investigated core morphology of the MA mutants by negative-stain electron microscopy. Preparations of WT particles contained cone-shaped mature cores as expected (Fig. 6A). The two MA mutants (V6R and L20K) as well as V6R/K97E also gave mature cores. Notably, we found that size (both width and length) of

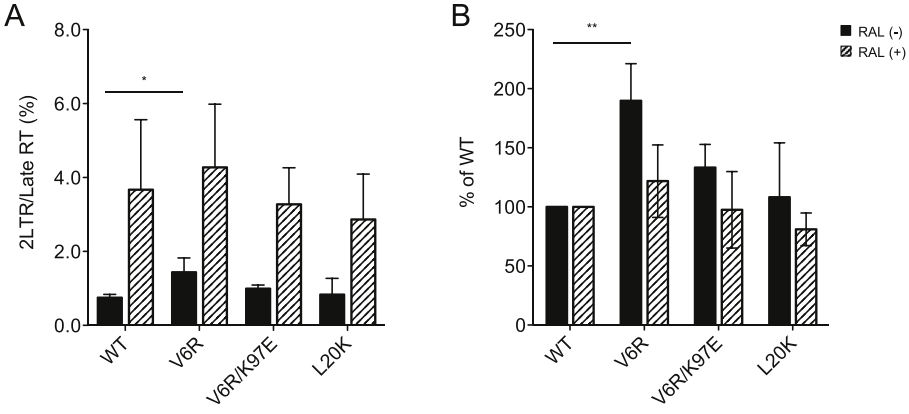

Fig. 4. Effect of HIV-1 MA mutations on 2-LTR formation in Jurkat cells. Jurkat cells were infected with VSV-G pseudotyped WT and MA mutant viruses in the absence or presence of 1 μM Raltegravir. The DNA was extracted at 24 h after infection and subjected to real-time PCR using 2-LTR primers for nuclear transported viral DNA. The level of each mutant is indicated by ratio of 2-LTR to late RT products (A) or relative to the average values of the WT virus, which was set as 100% (B). Error bars reflect the standard deviations of four independent experiments, respectively. Values are significantly different as follows: *, $P = 0.01$ to 0.05, **, $P = 0.001$ to 0.01.

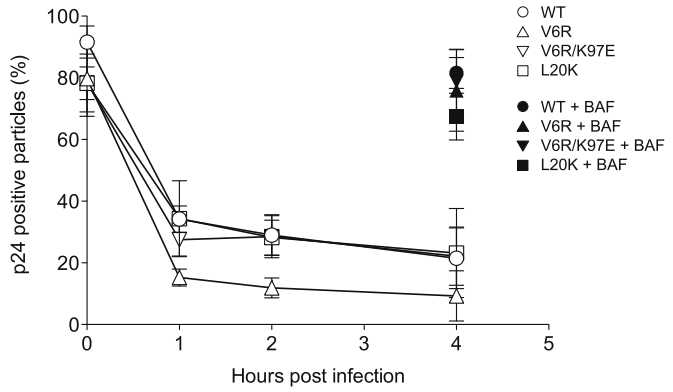

Fig. 5. *In situ* uncoating assay. *In situ* uncoating assay for WT and MA mutants was performed as described previously (ref.). Briefly, HeLa cells were spinoculated with fluorescently labled WT and MA mutant viruses containing GFP-Vpr or S15-dTomato for 2 h in the presence or absence of Bafilimycin A (BAF). At indicated times after the spinoculation, the infected cells were fixed, immunostained for p24 CA (Cy-5), and imaged. The total number of complexes that entered and fused into the cytoplasm (Vpr-GFP$^+$, S15-dTomato$^-$), the number of CA-coated complexes (Vpr-GFP$^+$, Ca-Cy5$^+$), and the number of CA-uncoated complexes that lost CA staining (Vpr-GFP$^+$, Ca-Cy5$^-$) were counted. The percentage of the total number of fused virions that stained p24 CA over time following fusion is shown. The 0 h time point and BAF (+) samples represent total number of GFP positive virions that stained positive for p24 CA. Results shown are the average of three independent experiments, with error bars representing standard deviations.

the V6R mutant was significantly bigger than that of WT (Fig. 6B), suggesting that mature core formation is affected by the V6R mutation.

3.6. Core stability in vitro is not affected by the V6R mutation

To investigate whether the V6R mutation intrinsically makes the viral cores unstable, we performed viral core isolation with "spin-thru" method and *in vitro* core disassembly assay using the isolated cores based on previous reports (Aiken, 2009; Forshey et al., 2002; Shah and Aiken, 2011). Using these methods, the cores were located in the fractions with densities between 1.23 and 1.27 g/ml, whereas intact virions were located in the fractions between 1.13 and 1.17 g/ml, which consistent with previous observations (Aiken, 2009; Forshey et al., 2002; Shah and Aiken, 2011). To validate the core isolation process, we first isolated viral cores from CA E128A/R132A and E45A mutants. Consistent with a previous report (Forshey et al., 2002), both CA mutants showed increased yields of the viral cores compared with that of WT (Fig. 7A and B). In this set of experiments for core isolation and *in vitro* core disassembly, we included two MA mutants, L7E and S8A, in addition to V6R, V6R/K97E and L20K. The L7E and S8A MA mutants, like V6R, exhibit decreased membrane binding and impaired Pr55^{Gag} processing (Ono and Freed, 1999). We observed that core density of the MA mutants analyzed in the present study is comparable to that of WT, suggesting that the numbers of CA proteins per unit volume of cores in the MA mutant were comparable to those of WT (Fig. 8A and B). The yields of viral cores of the MA mutants were comparable to those of WT except the L7E in which the core yield was about one-third to that of WT (Fig. 8B). Consistent with a previous study (Ono and Freed, 1999), L7E showed severe defects in viral release. This phenotype causes inaccuracy in normalization of input virions from the assay, leading to the observed results. Thus, the data may reflect limitations of the assay system rather than instability of the core. To directly assess the physical stability of the viral cores for the MA mutants, we performed an *in vitro*

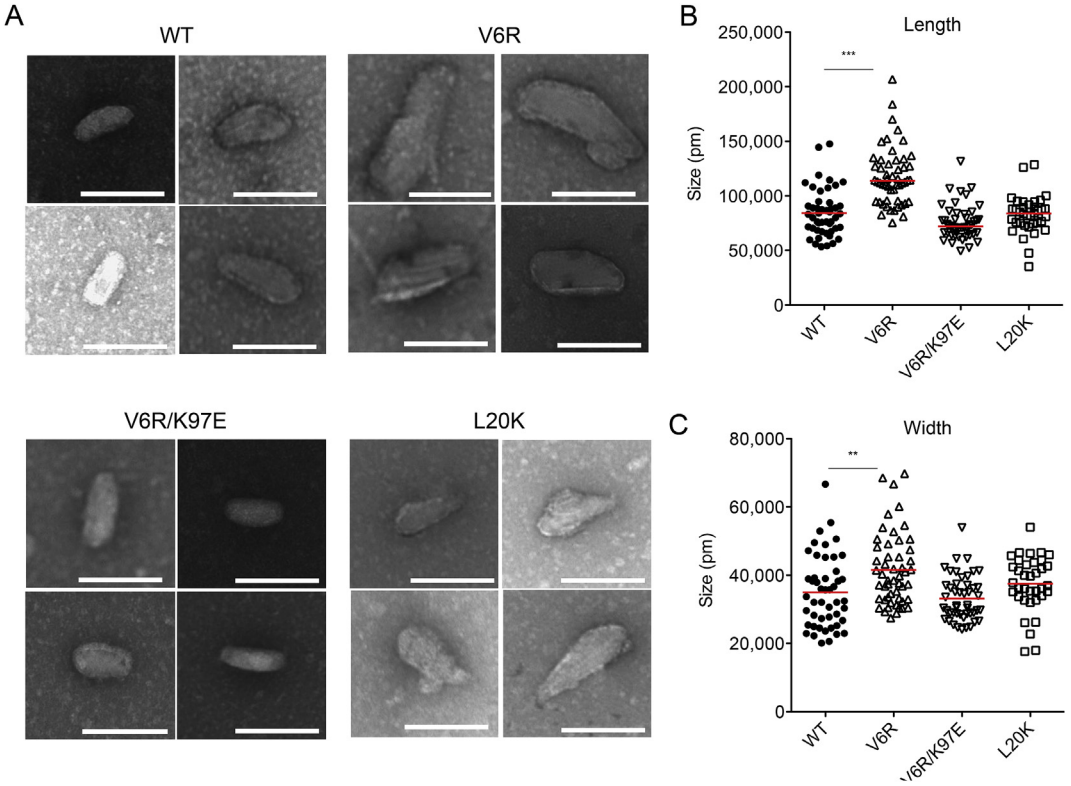

Fig. 6. Analysis of core morphology and sizes of WT and MA mutants cores. (A) Virions were treated with detergent and the cores were isolated and analyzed by negative-stained electron microscopy (EM). EM pictures are the representatives of observations performed on X to Y viral cores. The scale bars are 100 nm and identical for all images shown. The lengths (B) and widths (C) of at least 35 cores for WT and MA mutants for were measured. **, $P = 0.001$ to 0.01, ***, $P < 0.001$.

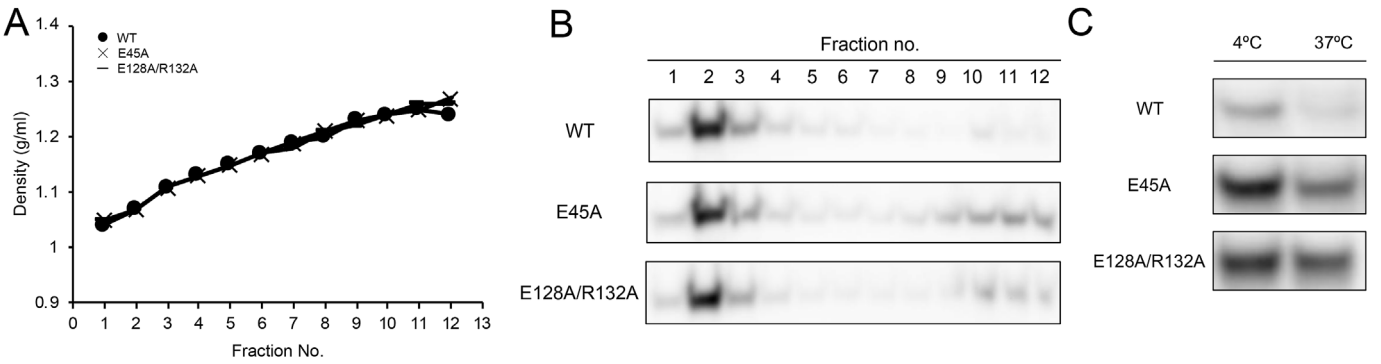

Fig. 7. Isolation and *in vitro* disassembly assay of HIV-1 cores of CA mutants. (A and B) equilibrium density gradient sedimentation of HIV-1 cores. Concentrated virions were layered onto 30–70% linear sucrose gradient with a layer of 1% Triton X-100. Following ultracentrifugation at 100, 000 × *g* for 18 h at 4 °C, fractions were collected from the top of the gradient and were analyzed by western blotting with the *anti*-p24 antibody. (C) The fractions containing HIV-1 cores (1.23–1.26 g/ml of density) were diluted and incubated for 2 h at 37 °C or 4 °C. Following incubation, the cores were centrifuged at 20,000 × *g* for 1.5 h at 4 °C. Data are representative of at least two independent experiments.

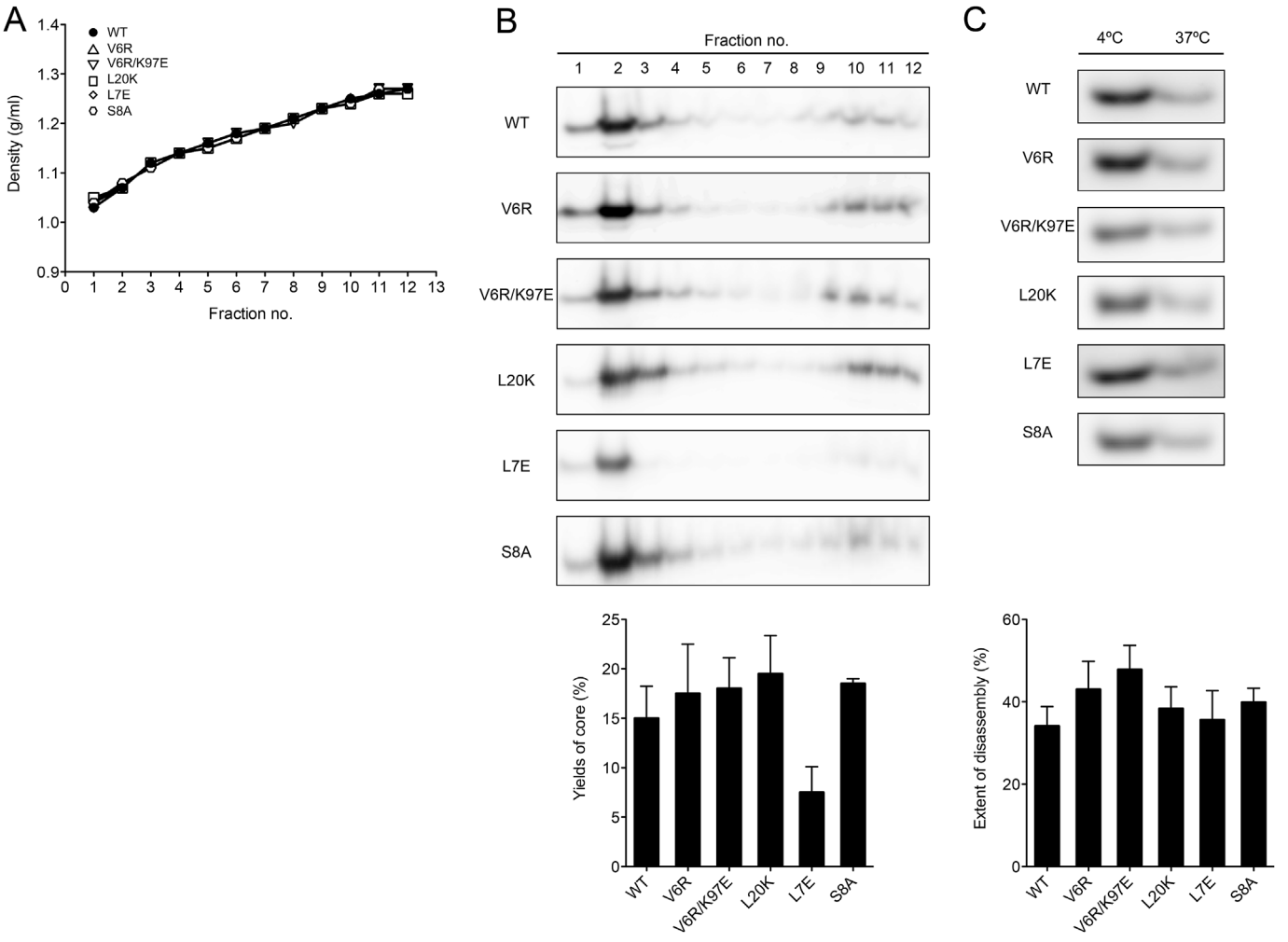

Fig. 8. Isolation and *in vitro* disassembly assay of MA mutant cores. (A) equilibrium density gradient sedimentation of HIV-1 cores. Concentrated virions were layered onto 30–70% linear sucrose gradient with a layer of 1% Triton X-100. Following ultracentrifugation at 100, 000 × *g* for 18 h at 4 °C, fractions were collected from the top of the gradient and were analyzed by western blotting with the *anti*-p24 antibody. The intensity of the bands was quantified by densitometry. (B) Yields of the isolated cores were calculated as the percentage of the total CA in the core fraction (1.23–1.26 g/ml). Upper panel is the representative data and lower panel shows the averages of at least three independent experiments, with error bars representing standard deviations. (C) The fractions containing HIV-1 cores (1.23–1.26 g/ml of density) were diluted and incubated for 2 h at 37 °C or 4 °C. Following incubation, the cores were centrifuged at 20,000 × *g* for 1.5 h at 4 °C. The ratio of pellet p24 amounts at 37 °C to that at 4 °C were shown. Upper panel is the representative data and lower panel shows the averages of at least three independent experiments with error bars representing standard deviations.

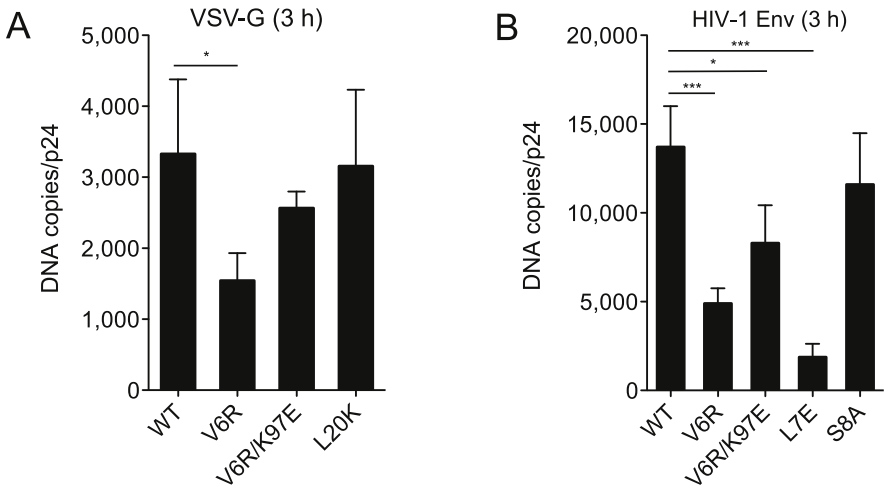

Fig. 9. Effect of MA mutations on the activity of natural ERT of (A) VSV-G pseudotyped HIV-1 or (B) HIV-1 infectious molecular clones. ERT reactions were initiated by the addition deoxyribonucleotides to DNase I-treated viruses containing 10 ng of p24 on ice. Following incubation at 37C, the reactions were terminated at 3 h after incubation. Viral DNA was extracted and measured for R/U5 DNA by quantitative real-time PCR analysis. Error bars reflect the standard errors (upper panels) and the standard deviations of at least three independent experiments, respectively. Values are significantly different as follows: *, P = 0.01 to 0.05, **, P = 0.001 to 0.01.

core disassembly assay. The fractions containing cores (1.23–1.27 g/ml) were diluted and incubated at 37 °C or 4 °C for 2 h. Following incubation, the cores were centrifuged at 4 °C at 20,000 × *g* for 90 min. To determine the core stability, pellet fractions were subjected to SDS-PAGE and Western blot analysis. In this assay, we again observed, consistent with the previous report (Forshey et al., 2002), that the CA E128A/R132A and E45A mutants increased core stability (Fig. 7C). Unexpectedly, all MA mutants including V6R demonstrated WT core stability to WT (Fig. 8C). These results suggest that the V6R mutation does not intrinsically make the viral cores unstable although this mutation accelerated the kinetics of uncoating in virus-infected cells (Fig. 5).

3.7. The V6R mutation impairs the initiation of reverse transcription in virions

We next examined whether the V6R mutation affects the initiation of reverse transcription (RT) in virus particles by endogenous RT (ERT) assays. We adopted the so-called “natural ERT assay” in which we did not add any detergent so that we could avoid the effect of detergent on the viral cores in the assay (Thomas et al., 2011; Warrilow et al., 2008). In the first set of experiment, we used VSV-G pseudotyped viruses that were used in most of the experiments. The V6R mutant showed impaired ERT activity whereas the V6R/K97E and L20K viruses showed comparable levels of the ERT activity (Fig. 9A). The HIV-1 envelope proteins (Env) are considered to play an important role in the permeability of virions to dNTPs (Zhang et al., 1996). To investigate the ERT activity of physiologically relevant virions, we also examined ERT activity for WT and MA mutants that have the HIV-1 Env in the second set of experiment. The V6R and L7E mutants showed impaired endogenous RT reaction whereas the revertant V6R/K97E partially restored endogenous RT reaction although the difference between V6R and the revertant is not statistically significant (Fig. 9B). The S8A mutant, which decreases the Gag membrane binding to a lesser extent than V6R and L7E (Ono and Freed, 1999), showed similar endogenous RT activity as WT. These results indicate that MA mutations such as the V6R, L7E, for which Gag membrane binding is drastically decreased, impair the initiation of the RT reaction in the virions regardless of the kinds of envelope proteins.

4. Discussion

It is well known that HIV-1 matrix (MA) has important roles for the late stages of the HIV-1 replication cycle, such as membrane binding and targeting of the Gag precursor proteins ($Pr55^{Gag}$) to the plasma membrane, and Env incorporation into the virion. However, impacts of MA mutants that alter the Gag membrane binding on the phenotypes of the newly produced virus particles have not been extensively examined. In the present study, we found that the V6R mutation in the HIV-1 MA N-terminus, which decreased membrane binding of Gag, increased the size of viral cores, accelerated uncoating in infected cells without decreased physical core stability, and impaired reverse transcription in infected cells. On the other hand, the level of the integrated DNA in infected cells was significantly decreased by the L20K mutation, although the mutation did not appear to affect the virion compositions or morphology. These results suggest that MA plays important roles in mature core formation and post-entry events in the HIV-1 replication cycle.

As observed in previous studies from the Freed lab (Freed et al., 1994; Ono et al., 1997; Ono and Freed, 1999), we confirmed that MA mutations analyzed in the present study did not affect the virion composition, vRNA encapsidation or Gag processing in the virions released from transfected 293T cells (Fig. 1). However, TEM analysis showed that the viral core of V6R was significantly larger than that of WT whereas that of V6R/K97E, a revertant for the V6R, was restored to WT level (Fig. 6). These results indicate that the HIV-1 MA is involved in core morphogenesis, which is a new finding in the HIV research field. Because core assembly is thought to be influenced by the size of the viral envelope membrane or the Gag sphere (Frank et al., 2015; Ning et al., 2016), it is possible that the V6R mutation modifies the physical properties of the core assembly elements. This in turn can influence the core maturation pathway through either the *de novo* reassembly model or displacive model (Briggs et al., 2009; Frank et al., 2015; Konvalinka et al., 2015; Ning et al., 2016; Woodward et al., 2015), resulting in enlarged sizes of mature cores. Further study is necessary to address each of these issues.

We assessed the viral core stability by two different techniques. *In vitro* disassembly assay indicated that the physical stability and density of V6R viral cores was comparable to that of WT (Fig. 8). In contrast, an *in situ* uncoating assay revealed that the V6R viral cores disassembled more rapidly in infected HeLa cells (Fig. 5). Although this apparent discrepancy remains to be clarified, it may be due to the lack of *trans*-acting factors in the physical stability assay. In this regard, several studies identified host factors that modulate viral uncoating of HIV (Chen et al., 2018). The V6R mutation may increase sensitivity to these host factors that modulate uncoating processes because of the increased size of viral cores.

Many lines of evidence have suggested that HIV-1 uncoating is linked to reverse transcription in the infected cells (Cosnefroy et al., 2016; Forshey et al., 2002; Hulme et al., 2011; Yang et al., 2013). A recent study indicated the early steps of HIV-1 reverse transcription is initiated inside the viral cores and these early reverse transcripts trigger

uncoating (Rankovic et al., 2017). Our study demonstrated that the V6R mutation decreased the efficiency of the reverse transcription both in the infected cells (Fig. 3) and in newly produced virions (Fig. 9), These results suggest that the V6R mutation affects the structural transition of the viral cores, resulting in defects in uncoating and reverse transcription in the next round of infection. Thus, the MA protein seems to play indirect roles in the early stages of the HIV-1 replication cycle.

Similar to the V6R mutation, VSV-G pseudotyped L20K also showed defects in single-cycle infectivity (Fig. 2). However, the impacts of the MA mutations on the post-entry steps seem to be different. Whereas the previous study indicated that the L20K mutant affected the reverse transcription in the infected cells and the ERT activity inside the viral cores (Kiernan et al., 1998), the present study showed that L20K did not affect HIV-1 cDNA synthesis (Fig. 3) or ERT activity (Fig. 9). The difference between the previous and present result may be due to the differences of methods used to analyze ERT activity or producer cell lines (HeLa versus 293T) in the ERT assays or target cell lines (CEM (12D7) versus Jurkat) in the case of viral cDNA synthesis measurements. In the present study, we assessed ERT activity without using detergents to avoid damaging the viral cores (Thomas et al., 2011; Warrilow et al., 2008). Under this condition, we can examine not only the initiation of reverse transcription, but also the integrity of the virions. Some reports have shown effects of producer cells on viral physiology (Iordanskiy et al., 2013). Although we confirmed the L20K mutation showed comparable phenotypes to WT with respect to the viral composition and morphology, we did not examine the incorporation of host factors that modulate viral core stability or initiation of reverse transcription in the virions.

Both the V6R and L20K decreased the integrated form of the HIV-1 DNA without affecting the efficiency of the nuclear import (Figs. 3 and 4). However, the mechanisms of decreased levels of the integrated DNA seem to be different between the two MA mutants. As observed with the HIV-1 integrase (IN) catalytic site mutants that abolish the IN function (Tsurutani et al., 2000), the V6R mutation increased the levels of 2-LTR, suggesting that the V6R mutation have any impact of the nuclear import of the viral DNA and/or the IN function in the nucleus. The level of 2-LTR formation of the V6R mutant was comparable to that of WT in the presence of RAL (Fig. 4), suggesting that the V6R mutation does not affect the nuclear import. Unlike the V6R, the L20K decreased the integrated DNA without increasing the 2-LTR forms, suggesting that the L20K mutation somehow decreases the stability of the viral cDNA rather than inhibiting the integration process itself. Whereas the majority of the HIV-1 MA is associated with the viral membrane, it has been reported that at least a part of the MA is associated with the viral cores or pre-integration complex (PIC) (Bukrinsky et al., 1993; Miller et al., 1997). In addition, biochemical analyses such as gel shift assay, NMR and isothermal titration calorimetry demonstrated the association of the HIV-1 MA with the viral DNA (Cai et al., 2010; Hearps et al., 2008). A recent report indicated that knockdown of a host protein LRPPRC, which was found to be associated with both the MA and IN of HIV-1, impaired the PIC formation in a certain cell type (Schweitzer et al., 2012). Thus, MA mutations such as the V6R and L20K that alter Gag membrane binding may affect the MA-PIC interaction and/or the interaction between the MA and host factors such as the LRPRRC mentioned above, resulting in changing the PIC stability and/or the following integration efficiency in the infected cells although further detailed studies must be performed to validate these possibilities.

In summary, we obtained new information and insights into the impact of MA mutations that alter Gag membrane binding on core morphogenesis and post-entry processes. The V6R MA mutation, which increases Gag membrane binding increased the sizes of mature cores, accelerated uncoating and impaired reverse transcription and integration. On the other hand, the L20K MA mutation, which decreases Gag membrane binding did not affect core morphogenesis but impaired HIV-1 integration. Our findings provide new and significant information on the roles of the HIV-1 MA in the virus replication cycle.

5. Conclusions

A mutation in the N-terminus of HIV-1 MA, V6R, which decreases membrane binding of Gag, increased the size of the mature cores. The V6R mutation accelerated uncoating, and impaired reverse transcription and integration steps in the next-round infection. On the other hand, a MA mutation in the highly basic patch, L20K, which increases membrane binding of Gag decreased the amount of integrated DNA in the infected cells. These results provide new insights into the roles of HIV-1 MA in viral core morphogenesis and post-entry events in the HIV-1 replication cycle.

Acknowledgements

We would like to thank Dr. T. Shioda and Dr. H. Sato for organizing the collaboration and their helpful discussion and comments on this study. We are grateful to Dr. E. O. Freed for his helpful discussion and comments on the manuscript, and providing us the plasmids of HIV-1 MA mutants. We thank Ms. H. Ohmori for her support with transmission electron microscopy analysis. We thank Dr. J. Sakuragi, Dr. T. Masuda, Dr. H. Takeuchi and Dr. H. Saito for helpful suggestions. We thank Dr. A. Adachi for H9/H1luc cell, Dr. J. Burns for plasmid pHCMV-G, and Dr. J. Chiba for 7C4 monoclonal antibody. The following reagents were obtained through the NIH AIDS Reagent Program, Division of AIDS, NIAID, NIH: TZM-bl from Dr. J. C. Kappes, Dr. X. Wu and Tranzyme Inc. *Anti*-HIV-1 HXB2 IN 1–16 aa Polyclonal (cat# 756) from Dr. D. P. Grandgenett. This study was mainly supported by grants to TM, and HS (Research on HIV/AIDS project no. H25-003 from the Ministry of Health, Labour and Welfare of Japan) and grants to TM, and HS from Japan Agency for Medical Research and Development, AMED (Research Program on HIV/AIDS: fund ID, 15fk0410009). This study was also supported by Joint Research Project of the Research Institute for Microbial Diseases, Osaka University (H26 and H27).

References

Accola, M.A., Ohagen, A., Göttlinger, H.G., 2000. Isolation of human immunodeficiency virus type 1 cores: retention of Vpr in the absence of p6 (gag). J. Virol. 74, 6198–6202.

Adachi, A., Gendelman, H.E., Koenig, S., Folks, T., Willey, R., Rabson, A., Martin, M.A., 1986. Production of acquired immunodeficiency syndrome-associated retrovirus in human and nonhuman cells transfected with an infectious molecular clone. J. Virol. 59, 284–291.

Aiken, C., 2009. Cell-free assays for HIV-1 uncoating. Methods Mol. Biol. 485, 41–53.

Aiken, C., 1997. Pseudotyping human immunodeficiency virus type 1 (HIV-1) by the glycoprotein of vesicular stomatitis virus targets HIV-1 entry to an endocytic pathway and suppresses both the requirement for Nef and the sensitivity to cyclosporin A. J. Virol. 71, 5871–5877.

Alfadhli, A., Barklis, R.L., Barklis, E., 2009. HIV-1 matrix organizes as a hexamer of trimers on membranes containing phosphatidylinositol-(4,5)-bisphosphate. Virology 387, 466–472.

Briggs, J.A.G., Riches, J.D., Glass, B., Bartonova, V., Zanetti, G., Krausslich, H.-G., 2009. Structure and assembly of immature HIV. Proc. Natl. Acad. Sci. U.S.A. 106, 11090–11095.

Bukrinsky, M.I., Sharova, N., McDonald, T.L., Pushkarskaya, T., Tarpley, W.G., Stevenson, M., 1993. Association of integrase, matrix, and reverse transcriptase antigens of human immunodeficiency virus type 1 with viral nucleic acids following acute infection. Proc. Natl. Acad. Sci. U.S.A. 90, 6125–6129.

Butler, S.L., Hansen, M.S.T., Bushman, F.D., 2001. A quantitative assay for HIV DNA integration in vivo. Nat. Med. 7, 631–634.

Cai, M., Huang, Y., Craigie, R., Clore, G.M., 2010. Structural basis of the association of HIV-1 matrix protein with DNA. PLoS One 5, 2–7.

Campbell, E.M., Perez, O., Melar, M., Hope, T.J., 2007. Labeling HIV-1 virions with two fluorescent proteins allows identification of virions that have productively entered the target cell. Virology 360, 286–293.

Chen, L., Keppler, O.T., Schölz, C., 2018. Post-translational modification-based regulation of HIV replication. Front. Microbiol. 9, 2131.

Chiba, J., Yamaguchi, A., Suzuki, Y., Nakano, M., Zhu, W., Ohba, H., Saito, A., Shinagawa, H., Yamakawa, Y., Kobayashi, T., Kurata, T., 1996. A novel neutralization epitope on the “thumb” subdomain of human immunodeficiency virus type 1 reverse transcriptase revealed by a monoclonal antibody. J. Gen. Virol. 77 (Pt 12), 2921–2929.

Cosnefroy, O., Murray, P.J., Bishop, K.N., 2016. HIV-1 capsid uncoating initiates after the first strand transfer of reverse transcription. Retrovirology 13, 58.

Dalton, A.K., Ako-Adjei, D., Murray, P.S., Murray, D., Vogt, V.M., 2007. Electrostatic interactions drive membrane association of the human immunodeficiency virus type

1 Gag MA domain. J. Virol. 81, 6434–6445.
Derdeyn, C. a, Decker, J.M., Sfakianos, J.N., Wu, X., O'Brien, W. a, Ratner, L., Kappes, J.C., Shaw, G.M., Hunter, E., 2000. Sensitivity of human immunodeficiency virus type 1 to the fusion inhibitor T-20 is modulated by coreceptor specificity defined by the V3 loop of gp120. J. Virol. 74, 8358–8367.
Forshey, B.M., von Schwedler, U., Sundquist, W.I., Aiken, C., 2002. Formation of a human immunodeficiency virus type 1 core of optimal stability is crucial for viral replication. J. Virol. 76, 5667–5677.
Frank, G.A., Narayan, K., Bess, J.W., Del Prete, G.Q., Wu, X., Moran, A., Hartnell, L.M., Earl, L.A., Lifson, J.D., Subramaniam, S., 2015. Maturation of the HIV-1 core by a non-diffusional phase transition. Nat. Commun. 8, 5864.
Freed, E.O., 2015. HIV-1 assembly, release and maturation. Nat. Rev. Microbiol. 13, 484–496.
Freed, E.O., Orenstein, J.M., Buckler-White, A.J., Martin, M.A., 1994. Single amino acid changes in the human immunodeficiency virus type 1 matrix protein block virus particle production. J. Virol. 68, 5311–5320.
Grandgenett, D.P., Goodarzi, G., 2008. Folding of the multidomain human immunodeficiency virus type-I integrase. Protein Sci. 3, 888–897.
Hearps, A.C., Wagstaff, K.M., Piller, S.C., Jans, D.A., 2008. The N-terminal basic domain of the HIV-1 matrix protein does not contain a conventional nuclear localization sequence but is required for DNA binding and protein self-association. Biochemistry 47, 2199–2210.
Hill, C.P., Worthylake, D., Bancroft, D.P., Christensen, A.M., Sundquist, W.I., 1996. Crystal structures of the trimeric human immunodeficiency virus type 1 matrix protein: implications for membrane association and assembly. Proc. Natl. Acad. Sci. U.S.A. 93, 3099–3104.
Hori, T., Takeuchi, H., Saito, H., Sakuma, R., Inagaki, Y., Yamaoka, S., 2013. A carboxy-terminally truncated human CPSF6 lacking residues encoded by exon 6 inhibits HIV-1 cDNA synthesis and promotes capsid disassembly. J. Virol. 87, 7726–7736.
Hulme, A.E., Perez, O., Hope, T.J., 2011. Complementary assays reveal a relationship between HIV-1 uncoating and reverse transcription. Proc. Natl. Acad. Sci. U.S.A. 108, 9975–9980.
Iordanskiy, S., Santos, S., Bukrinsky, M., 2013. Nature, nurture and HIV: the effect of producer cell on viral physiology. Virology 443, 208–213.
J Buzón, M., Massanella, M., Llibre, J.M., Esteve, A., Dahl, V., Puertas, M.C., Gatell, J.M., Domingo, P., Paredes, R., Sharkey, M., Palmer, S., Stevenson, M., Clotet, B., Blanco, J., Martinez-Picado, J., 2010. HIV-1 replication and immune dynamics are affected by raltegravir intensification of HAART-suppressed subjects. Nat. Med. 16, 460–465.
Kiernan, R.E., Ono, A., Englund, G., Freed, E.O., 1998. Role of matrix in an early post-entry step in the human immunodeficiency virus type 1 life cycle. J. Virol. 72, 4116–4126.
Kono, K., Takeda, E., Tsutsui, H., Kuroishi, A., Hulme, A.E., Hope, T.J., Nakayama, E.E., Shioda, T., 2013. Slower uncoating is associated with impaired replicative capability of simian-tropic HIV-1. PLoS One 8, e72531.
Konvalinka, J., Kräusslich, H.-G., Müller, B., 2015. Retroviral proteases and their roles in virion maturation. Virology 479–480, 403–417.
Lingappa, J.R., Reed, J.C., Tanaka, M., Chutiraka, K., Robinson, B.A., 2014. How HIV-1 Gag assembles in cells: putting together pieces of the puzzle. Virus Res. 193, 89–107.
Massiah, M.A., Starich, M.R., Paschall, C., Summers, M.F., Christensen, A.M., Sundquist, W.I., 1994. Three-dimensional structure of the human immunodeficiency virus type 1 matrix protein. J. Mol. Biol. 244, 198–223.
Miller, M.D., Farnet, C.M., Bushman, F.D., 1997. Human immunodeficiency virus type 1 preintegration complexes: studies of organization and composition. J. Virol. 71, 5382–5390.
Nagao, T., Yoshida, A., Sakurai, A., Piroozmand, A., Jere, A., Fujita, M., Uchiyama, T., Adachi, A., 2004. Determination of HIV-1 infectivity by lymphocytic cell lines with integrated luciferase gene. Int. J. Mol. Med. 14, 1073–1076.
Ning, J., Erdemci-Tandogan, G., Yufenyuy, E.L., Wagner, J., Himes, B.A., Zhao, G., Aiken, C., Zandi, R., Zhang, P., 2016. In vitro protease cleavage and computer simulations reveal the HIV-1 capsid maturation pathway. Nat. Commun. 7, 13689.
Ohishi, M., Nakano, T., Sakuragi, S., Shioda, T., Sano, K., Sakuragi, J. -i., 2011. The relationship between HIV-1 genome RNA dimerization, virion maturation and infectivity. Nucleic Acids Res. 39, 3404–3417.
Ohishi, M., Shioda, T., Sakuragi, J., 2007. Retro-transduction by virus pseudotyped with glycoprotein of vesicular stomatitis virus. Virology 362, 131–138.
Ono, A., Freed, E.O., 1999. Binding of human immunodeficiency virus type 1 Gag to membrane: role of the matrix amino terminus. J. Virol. 73, 4136–4144.
Ono, A., Huang, M., Freed, E.O., 1997. Characterization of human immunodeficiency virus type 1 matrix revertants: effects on virus assembly, Gag processing, and Env incorporation into virions. J. Virol. 71, 4409–4418.
Ono, A., Orenstein, J.M., Freed, E.O., 2000. Role of the Gag matrix domain in targeting human immunodeficiency virus type 1 assembly. J. Virol. 74, 2855–2866.
Ono, A., Ablan, S.D., Lockett, S.J., Nagashima, K., Freed, E.O., 2004. Phosphatidylinositol (4,5) bisphosphate regulates HIV-1 Gag targeting to the plasma membrane. Proc. Natl. Acad. Sci. U.S.A. 101, 14889–14894.
Platt, E.J., Bilska, M., Kozak, S.L., Kabat, D., Montefiori, D.C., 2009. Evidence that ecotropic murine leukemia virus contamination in TZM-bl cells does not affect the outcome of neutralizing antibody assays with human immunodeficiency virus type 1. J. Virol. 83, 8289–8292.
Platt, E.J., Wehrly, K., Kuhmann, S.E., Chesebro, B., Kabat, D., 1998. Effects of CCR5 and CD4 cell surface concentrations on infections by macrophagetropic isolates of human immunodeficiency virus type 1. J. Virol. 72, 2855–2864.
Rankovic, S., Varadarajan, J., Ramalho, R., Aiken, C., Rousso, I., 2017. Reverse transcription mechanically initiates HIV-1 capsid disassembly. J. Virol. 91 e00289-17.
Robinson, B.A., Reed, J.C., Geary, C.D., Swain, J.V., Lingappa, J.R., 2014. A temporospatial map that defines specific steps at which critical surfaces in the Gag MA and CA domains act during immature HIV-1 capsid assembly in cells. J. Virol. 88, 5718–5741.
Saad, J.S., Loeliger, E., Luncsford, P., Liriano, M., Tai, J., Kim, A., Miller, J., Joshi, A., Freed, E.O., Summers, M.F., 2007. Point mutations in the HIV-1 matrix protein turn off the myristyl switch. J. Mol. Biol. 366, 574–585.
Saad, J.S., Miller, J., Tai, J., Kim, A., Ghanam, R.H., Summers, M.F., 2006. Structural basis for targeting HIV-1 Gag proteins to the plasma membrane for virus assembly. Proc. Natl. Acad. Sci. U.S.A. 103, 11364–11369.
Sakuragi, J.-I., Ueda, S., Iwamoto, A., Shioda, T., 2003. Possible role of dimerization in human immunodeficiency virus type 1 genome RNA packaging. J. Virol. 77, 4060–4069.
Schweitzer, C.J., Matthews, J.M., Madson, C.J., Donnellan, M.R., Cerny, R.L., Belshan, M., 2012. Knockdown of the cellular protein LRPPRC attenuates HIV-1 infection. PLoS One 7, e40537.
Shah, V.B., Aiken, C., 2011. In vitro uncoating of HIV-1 cores. JoVE 57.
Suzuki, Y., Misawa, N., Sato, C., Ebina, H., Masuda, T., Yamamoto, N., Koyanagi, Y., 2003. Quantitative analysis of human immunodeficiency virus type 1 DNA dynamics by real-time PCR: integration efficiency in stimulated and unstimulated peripheral blood mononuclear cells. Virus Gene. 27, 177–188.
Svarovskaia, E.S., Barr, R., Zhang, X., Pais, G.C.G., Marchand, C., Pommier, Y., Burke, T.R., Pathak, V.K., Pathak, V.K., 2004. Azido-containing diketo acid derivatives inhibit human immunodeficiency virus type 1 integrase in vivo and influence the frequency of deletions at two-long-terminal-repeat-circle junctions. J. Virol. 78, 3210–3222.
Takeuchi, Y., McClure, M.O., Pizzato, M., 2008. Identification of gammaretroviruses constitutively released from cell lines used for human immunodeficiency virus research. J. Virol. 82, 12585–12588.
Tanaka, M., Robinson, B.A., Chutiraka, K., Geary, C.D., Reed, J.C., Lingappa, J.R., 2016. Mutations of conserved residues in the major homology region arrest assembling HIV-1 Gag as a membrane-targeted intermediate containing Genomic RNA and Cellular Proteins. J. Virol. 90, 1944–1963.
Tang, C., Loeliger, E., Luncsford, P., Kinde, I., Beckett, D., Summers, M.F., 2004. Entropic switch regulates myristate exposure in the HIV-1 matrix protein. Proc. Natl. Acad. Sci. U.S.A. 101, 517–522.
Tedbury, P.R., Mercredi, P.Y., Gaines, C.R., Summers, M.F., Freed, E.O., 2015. Elucidating the mechanism by which compensatory mutations rescue an HIV-1 matrix mutant defective for gag membrane targeting and envelope glycoprotein incorporation. J. Mol. Biol. 427, 1413–1427.
Tedbury, P.R., Novikova, M., Ablan, S.D., Freed, E.O., 2016. Biochemical evidence of a role for matrix trimerization in HIV-1 envelope glycoprotein incorporation. Proc. Natl. Acad. Sci. U.S.A. 113, E182–E190.
Thomas, J.A., Shatzer, T.L., Gorelick, R.J., 2011. Blocking premature reverse transcription fails to rescue the HIV-1 nucleocapsid-mutant replication defect. Retrovirology 8, 46.
Tsurutani, N., Kubo, M., Maeda, Y., Ohashi, T., Yamamoto, N., Kannagi, M., Masuda, T., 2000. Identification of critical amino acid residues in human immunodeficiency virus type 1 IN required for efficient proviral DNA formation at steps prior to integration in dividing and nondividing cells. J. Virol. 74, 4795–4806.
von Schwedler, U.K., Stray, K.M., Garrus, J.E., Sundquist, W.I., 2003. Functional Surfaces of the human immunodeficiency virus type 1 capsid protein. J. Virol. 77, 5439–5450.
Warrilow, D., Meredith, L., Davis, A., Burrell, C., Li, P., Harrich, D., 2008. Cell factors stimulate human immunodeficiency virus type 1 reverse transcription in vitro. J. Virol. 82, 1425–1437.
Wei, X., Decker, J.M., Liu, H., Zhang, Z., Arani, R.B., Kilby, J.M., Saag, M.S., Wu, X., Shaw, G.M., Kappes, J.C., 2002. Emergence of resistant human immunodeficiency virus type 1 in patients receiving fusion inhibitor (T-20) monotherapy. Antimicrob. Agents Chemother. 46, 1896–1906.
Willey, R.L., Smith, D.H., Lasky, L.A., Theodore, T.S., Earl, P.L., Moss, B., Capon, D.J., Martin, M.A., 1988. In vitro mutagenesis identifies a region within the envelope gene of the human immunodeficiency virus that is critical for infectivity. J. Virol. 62, 139–147.
Woodward, C.L., Cheng, S.N., Jensen, G.J., 2015. Electron cryotomography studies of maturing HIV-1 particles reveal the assembly pathway of the viral core. J. Virol. 89, 1267–1277.
Yamashita, M., Perez, O., Hope, T.J., Emerman, M., 2007. Evidence for direct involvement of the capsid protein in HIV infection of nondividing cells. PLoS Pathog. 3, 1502–1510.
Yang, Y., Fricke, T., Diaz-Griffero, F., 2013. Inhibition of reverse transcriptase activity increases stability of the HIV-1 core. J. Virol. 87, 683–687.
Yee, J.K., Miyanohara, A., LaPorte, P., Bouic, K., Burns, J.C., Friedmann, T., 1994. A general method for the generation of high-titer, pantropic retroviral vectors: highly efficient infection of primary hepatocytes. Proc. Natl. Acad. Sci. U.S.A. 91, 9564–9568.
Zhang, H., Dornadula, G., Alur, P., Laughlin, M.A., Pomerantz, R.J., 1996. Amphipathic domains in the C terminus of the transmembrane protein (gp41) permeabilize HIV-1 virions: a molecular mechanism underlying natural endogenous reverse transcription. Proc. Natl. Acad. Sci. U.S.A. 93, 12519–12524.